Published in final edited form as:
Biomacromolecules. 2013 May 13; 14(5): . doi:10.1021/bm400316e.

Biomimetic silicification of demineralized hierarchical collagenous tissues

Li-na Niu[#a], **Kai Jiao**[#a], **Heonjune Ryou**[b], **Anibal Diogenes**[c], **Cynthia K.Y. Yiu**[d], **Annalisa Mazzoni**[e], **Ji-hua Chen**[a,*], **Dwayne D. Arola**[b], **Kenneth M. Hargreaves**[c], **David H. Pashley**[f], and **Franklin R. Tay**[f,*]

[a]Fourth Military Medical University, Xi'an, China

[b]University of Maryland Baltimore County, Baltimore, Maryland, USA

[c]University of Texas Health Sciences Center at San Antonio, San Antonio, Texas, USA

[d]The University of Hong Kong, Hong Kong SAR, China

[e]University of Bologna, Bologna, Italy

[f]Georgia Regents University, Augusta, Georgia, USA

[#] These authors contributed equally to this work.

Abstract

Unlike man-made composite materials, natural biominerals containing composites usually demonstrate different levels of sophisticated hierarchical structures which are responsible for their mechanical properties and other metabolic functions. However, the complex spatial organizations of the organic-inorganic phases are far beyond what they be achieved by contemporary engineering techniques. Here, we demonstrate that carbonated apatite present in collagen matrices derived from fish scale and bovine bone may be replaced by amorphous silica, using an approach that simulates what is utilized by phylogenetically ancient glass sponges. The structural hierarchy of these collagen-based biomaterials is replicated by the infiltration and condensation of fluidic polymer-stabilized silicic acid precursors within the intrafibrillar milieu of type I collagen fibrils. This facile biomimetic silicification strategy may be used for fabricating silica-based, three-dimensional functional materials with specific morphological and hierarchical requirements.

Keywords

Biomimetic silicification; Calcification; Collagen; Hierarchical; Intrafibrillar

[*]**Corresponding Author** Franklin R. Tay, Georgia Regents University, Augusta, Georgia, 30912-1129, USA. TEL: (706) 7212031; tayfranklin7@gmail.com; Ji-hua Chen, School of Stomatology, Fourth Military Medical University, Xi'an, China; jhchen@fmmu.edu.cn.

Supporting Information. The detailed information about the analytical methods used in this work, the particle size distribution and zeta potential of the PAH-stabilized silicic acid, the TEM examination of natural fish scale, collagen sponges silicified without poly-allylamine and silicified of bovine trabecular bone, the SEM examination of sintered, silicified fish scales and additional references can be found in Supporting Information. This material is available free of charge via the Internet at http://pubs.acs.org.

Author Contributions The manuscript was written through contributions of all authors. All authors have given approval to the final version of the manuscript.

Notes The authors declare no competing financial interest.

1.INTRODUCTION

As the predominant biomineralization processes in Nature, calcified and silicified hard tissues share common motifs in terms of utilization of mineralization templates and mineralization mechanisms.[1-5] Because of its hierarchical tertiary structure and biocompatibility, type I collagen has been used repeatedly as templates for creating organic-inorganic hybrid materials with three-dimensional structural hierarchy.[1,4,6,7] Both biomimetic intrafibrillar calcification and intrafibrillar silicification of reconstituted type I collagen have recently been achieved *in vitro*.[7-9] Unlike reconstituted collagen, natural collagen/mineral biocomposites possess much higher strength and toughness due to the presence of different levels of hierarchy in the organic component, ranging from the nanoscale to the macroscale.[4] Thus, using the hierarchical structure of natural materials as a template for the development of new types of high-performance engineering materials is a promising approach.[10-12] Investigation of the silicification potential of naturally-calcified collagen matrices further broadens our overall appreciation of the possible existence of a unified biomineralization game plan in biomineralization. Here, by taking advantages of the biogenic hierarchical structures of the fish scale and bovine bone collagen matrices, we produced novel collagen-silica composites with unique hierarchical structures, via a polyamine-induced liquid precursor process.

Fish scale and bone are examples of hierarchically arranged nanocomposites, in which the collagen matrices are strengthened by intrafibrillar calcium-deficient apatite.[13,14] The alignment of collagen fibrils in the internal plies of fish scales is consistent within each individual ply, but varies from ply to ply, forming an orthogonal plywood structure (Supporting Information S2).[13,15,16] This hierarchical ply motif of fibrillar arrangement is also found in the basal spicules of some marine glass sponges, although the collagen composition in those sponges is different from type I collagen.[17] The light, flexible, tough and fracture-resistant properties of the fish scale have been a source of inspiration for materials scientists and armor engineers.[13,18] Bone forms the major mechanism of support in vertebrates, and represents an evolutionary advanced form of calcium phosphate biomineralization. The organic-inorganic components in bone tissues are arranged into six hierarchical levels.[14] Similarly, seven levels of hierarchical arrangement between silica and the organic matrix, from the nanometer to macroscopic length scales, are also found in hexactinellid sponges of the genus *Euplectella*.[19] In the present study, cycloid scales from *Cyprinus carpio* (the common fresh water carp) and bovine rib bone, in which these structural hierarchies are retained after delipidation and demineralization, serve as dense, natural collagen templates for biomimetic silicification. The hypothesis tested is that the naturally-calcified fish scale and bone collagen matrix can be intrafibrillarly silicified, with retention of the orginial hierachical arrangements of the collagen matrix.

2. EXPERIMENTAL SECTION

2.1.1 Preparation of poly(allylamine hydrochloride)-stabilized silicic acid precursors

A 10% silicic acid stock solution was prepared by mixing Silbond® 40 (40% hydrolyzed tetraethyl orthosilicate; TEOS; Silbond Corp., Weston, MI, USA), absolute ethanol, water and 37% HCl in the molar ratios of 1.875 : 93 : 12.03 : 0.0218 (mass ratio 15 : 42.84 : 2.167 : 0.008) for 1 hour at room temperature to complete the hydrolysis of TEOS into orthosilicic acid and its oligomers. The 10% silicic acid solution was then mixed with different concentrations of poly(allylamine hydrochloride) solution (PAH, average Mw 15,000; Sigma-Aldrich, St. Louis, MO, USA) in a 1:1 volume ratio, under vibration for 1 min, to obtain 5% silicic acid solutions that were stabilized by 0 mM, 0.083 mM, 0.167 mM, 0.333 mM, 0.667 mM, 1.333 mM and 2.667 mM PAH, respectively. The pH value of each solution was adjusted to 5 with 1 N HCl over 30-60 sec using predetermined volumes of the

acid. After centrifuging the mixture at 3000 RPM, the PAH-stabilized silicic acid (PAH-SA) was collected for turbidity assessment at different time points (0, 0.5, 1, 3, 6, 12, 24, 48, 72 and 96 hours). The concentration of PAH used for subsequent experiments was based on the minimal amount of PAH required for the solution to remain stable and visibly clear for at least 48 hours. This was monitored with optical density measurements taken at different time intervals, with a 96-well plate reader, at 405 nm. The optimal concentration of PAH for stabilizing the silicic acid was adopted for subsequent biomimetic silicification experiments. The particle size distribution and zeta potential measurement of PAH-SA were measured using a Zetatrac Particle Size Analyzer.

2.1.2 Silicification of reconstituted collagen sponges

The feasibility of the silicification strategy was first evaluated using reconstituted type I collagen sponges derived from bovine skin. Sponges (2 × 2 × 0.2 cm) were cut from reconstituted type I collagen tapes (Ace Surgical Supply Co., Inc, MA, USA). They were pre-washed, expanded with Milli-Q water (18.2 mΩ-cm), and silicified in 1 mL of 5% silicic acid (SA, control) or PAH-SA at 37 °C for 2 days, with daily change of the freshly prepared silicifying medium. The silicified collagen sponges were thoroughly rinsed with Milli-Q water for 10 times (5 min each) and prepared for TEM.

2.1.3 Silicification of *Cyprinus carpio* scale and bovine bone

Scales from a single wild-caught fresh water carp (*C. carpio*) were obtained from regions adjacent to the mid-length (beneath the dorsal fin). The scales were between 15 and 20 mm in diameter and less than 1 mm thick. Bovine rib bone was obtained from a local abattoir. The fish scales were sectioned into strips of 15 mm in length and 5 mm in width through the central part of the scale, and bone specimens were sectioned into 5 × 5 × 5 mm cubes, using a low-speed Isomet saw (Buehler, Lake Bluff, IL, USA), under water cooling. The fish scales were washed with 10 wt% NaCl solution for 1 day to remove surplus proteins, and completely demineralized with 0.5 M EDTA (pH 8) under continuous stirring for 1 week. The bone specimens were first delipidated in a mixture of chloroform and methanol (3:1 v/v), vigorously shaken for 3 days, and completely demineralized with 0.5 M EDTA for 2 weeks. The end point of demineralization was assessed by dropwise addition of a 30% potassium oxalate solution to the demineralization medium, which forms a white calcium oxalate precipitate when calcium ions are present. After the fish scales and bone specimens were completely demineralized, they were washed three times with deionized water to remove the EDTA, and immersed in a solution containing 4 M guanidine HCl, 60 mM Tris HCl (pH 7.0) at 4 °C for 24 h to extract bound noncollagenous proteins. The demineralized collagen matrices were incubated in the PAH-SA solution consisting of 5% of silicic acid and 0.667 mM of PAH for 7 days for the bone specimens, and 10 days for the fish scale specimens, with daily change of the freshly prepared silicifying medium.

2.1.4 Analytical methods

The analytical methods used in this work include transmission electron microscopy (TEM), scanning electron microscopy (SEM), attenuated total reflection–Fourier transform infrared spectroscopy (ATR-FTIR), scanning transmission electron microscopy-energy dispersive X-ray analysis (STEM-EDX), micro-computed tomography (micro-CT), solid-state nuclear magnetic resonance spectroscopy (NMR), powder X-ray diffraction (XRD), thermogravimetric analysis (TGA) and nanoscopical dynamic mechanical analysis (nanoDMA). Full experimental details are given in the Supporting Information S1.

3. RESULTS AND DISCUSSION

The proof-of-concept for the feasibility of intrafibrillar silicification has been accomplished by using a two-step technique.[9] This technique requires first treating reconstituted collagen fibrils with poly(allylamine) (PAH). This is followed by the use of the PAH-enriched collagen template for infiltration and coalescence of fluidic silicic acid nanoparticles (1.5% choline-stabilized silicic acid) within the intrafibrillar water compartments of the fibril. Unlike highly-porous reconstituted collagen scaffolds, both the collagen matrices of fish scales and bovine bone are very dense, which results in inadequate infiltration of the silica precursors. Thus, we developed a single-step biomimetic silicification scheme, using 0.667 mM PAH stabilized 5% silicic acid (PAH-SA) as silicification precursors (Supporting Information S3-A, Fig.S3-A). This novel protocol presents a more efficient method for the PAH-SA to infiltrate dense, natural collagen matrices. The mean particle diameter of the PAH-SA was ~142.2±18.7 nm, and the mean zeta potential was 39.4±3.0 mV (Supporting Information S3-B). The PAH appeared to stabilize polysilicic acid by preventing it from continuing polycondensation into silica particles outside the collagen fibrils, while maintaining the polysilicic acid in a fluidic state. The fluidic nature of the PAH-SA and the feasibility of the silicification strategy were first confirmed using reconstituted collagen sponges (Fig.1). The PAH-SA precursors attached initially to the surface of the collagen fibrils and subsequently infiltrated the fibrils. The fluidic nature of the PAH-SA precursors enabled them to assume the shape of the intrafibrillar space of the collagen fibrils, and formed intrafibrillar biominerals that reproduced the collagen tertiary architecture. Without PAH, the use of 5% silicic acid (SA control) resulted in the formation of silica particles on the surface of the collagen fibrils (Supporting Information S4 – Control I). The process of fluidic silicic acid infiltration via PAHstabilization is analogous to the use of a polymer-induced liquid precursor mechanism in the formation of calcium-based biominerals.[5]

Demineralized fish scales became highly silicified after incubation in PAH-SA for 10 days (Figs.2a and b). Electron-dense minerals were identified both in the extrafibrillar and intrafibrillar spaces. Unstained TEM image of longitudinally-arranged collagen fibrils from a single ply revealed electron-dense intrafibrillar silica deposits that replicated the D-spacing (67 nm) seen in stained fibrillar collagen (Fig.2c). These intrafibrillar silica deposits were clearly identified from cross-sections of collagen fibrils in the adjacent ply (Fig.2d). Fluidic PAH-SA nanoparticles were presumably transported into the closely approximated collagen fibrils through transversal canals and perpendicular sheet-like fibers (Fig.2b) that functioned as channels for transportation of calcium phosphate precursors during natural biocalcification of the fish scales. Removal of the organic components at high temperature produced inorganic silica replicas that resembled the plywood texture of natural scales, with ceramic-like, nanocrystalline characteristics (Supporting Information S5). Calcination performed at 700 °C resulted in fusion of the amorphous silica nanoparticles and their conversion into crystalline phases. For comparison, demineralized fish scales that were silicified with 5% silicic acid only in the absence of PAH (SA control) show silica particles depositing predominnatly on the surface of the fish scale. Although there was some infiltration of the silicic acid into the collagen matrix via the transversal canals, deposition of silica particles was extrafibrillar in nature, between the collagen fibrils (Supporting Information S6 – Control II).

Attenuated total reflection-Fourier transform infrared spectroscopy of natural fish scales (Fig.3a) revealed collagen-associated peaks and apatite-associated peaks.[16] Peaks at ~1650, 1550 and 1250 cm^{-1} (red arrows) are assigned respectively to the amide I (C=O stretch), amide II (NH bend coupled with CN stretch) and amide III (NH bend coupled with CN stretch) bands of type I collagen.[20] The peak at 1020 cm^{-1} is assigned to the $\nu 3PO_4$ stretching mode of hydroxyapatite. Peaks at 602 and 562 cm^{-1} are assigned to the $\nu 2$ and $\nu 4$

O-P-O bending modes of hydroxyapatite, respectively.[21] The peak at 1413 cm^{-1} (black arrows) is assigned to the ν3 C-O stretching mode of carbonate substitution in the apatite lattice.[21] After silicification, Si-OH vibration peak was identified near 940-960 cm^{-1} [22] and three main peaks characteristic of Si-O-Si vibrational modeswere detected at ≈460, 800 and 1070 cm^{-1}, respectively (Fig.3b).[23] The lowest frequency mode (~460 cm^{-1}) is assigned to transverse optical rocking motions (TO1 mode). Near 800 cm^{-1}, a weak band due to Si-O-Si symmetric stretching (TO2 mode) can be observed. The highest frequency mode around 1070 cm^{-1} is assigned to the anti-symmetric stretching of the Si-O-Si bonds (TO3 mode).[23] After sintering of the silicified fish scales, the Si-OH vibration peak disappeared due to total conversion of surface silanol groups to siloxane bonds. By using this silicification strategy, silicified fish scales may be functionalized by grafting different functional groups to their active surface silanol groups,[24] thereby providing an alternative method for fabricating functionalized silica-based materials with specific morphologic and hierarchy requirements. Alternatively, the collagen components can be dissolved in specific solvents at ambient temperature to generate mesoporous siliceous tissue engineering constructs for delivery of growth factors.

Compared to fish scale collagen, demineralized bone collagen matrix is less dense and is evenly silicified with PAH-SA after 7 days. Unstained TEM of silicified cortical bone (Fig. 4) and silicified trabecular bone (Supporting Information S7) show various hierarchical levels being replicated using demineralized bone collagen matrices and PAH-SA as building blocks. Fluidic PAH-SA was presumably delivered via the Haversian canal in the centre of the osteon and its interconnecting branches (Fig.4). Elemental mappings of non-osmicated specimens using STEM-EDX confirmed the presence of intrafibrillar silicon (Fig.4c) and oxygen (Fig.4d) within the silicified bone matrix. Micro-CT examination of bulk silicified bovine bone specimens indicates even silicification of both cortical and trabecular bone (Fig. 5). A movie prepared from the 3-D reconstructed images visibly could be found in the Supporting Information S8, showing that the entire piece of the demineralized bone matrix was silicified.

The extent of silica condensation within the silicified bone was identified using solid-state $^{1}H \rightarrow ^{29}Si$ cross polarization-magic angle spinning nuclear magnetic resonance spectroscopy. Both Q3 (single silanol) and Q4 (bulk siloxane) species were identified (Fig. 6a). Absence of Q2 (germinal silanol) and Q1 (silicic acid) species indicated high degree of condensation from silicic acid precursors to amorphous silica. Powder X-ray diffraction of silicified bone showed that the infiltrated mineral phase was amorphous (Fig.6b). After sintering of the silicified bone, the predominant crystalline silica phase was α–cristabolite. Thermogravimetric analyses comparing calcified bone with silicified bone are shown in Fig. 7. Whereas completely demineralized bone contains no minerals after sintering (Supporting Information S9), the lower mineral content of silicified bone (57.9 wt%) compared with calcified bone (65.2 wt%) may be caused by the lower density of silica compared with that of hydroxyapatite. Derivative weight loss from calcified bone indicated that sample lost weight in three steps: 20-160°C, attributed to evaporation of bound water from the organic matrix; 200-500 °C, attributed to pyrolysis of organic matter, and 700-900 °C, attributed to release of CO_2 from carbonated apatite.[25] For silicified bone, three desorption processes were observed: physisorbed water (peak at 71.4 °C), hydrogen-bonded structural water attributed to condensation of surface hydroxyl groups (peak at 288.5 °C), and decomposition of the organic matrix (peak at 364.3 °C). Absence of the peak at 853.3 °C in silicified bone indicates complete decalcification of the sample prior to biomimetic silicification (i.e. absence of carbonated apatite).

The literature is rich in evidence demonstrating the mineralization-templating function of collagen in both biocalcification and biosilicification,[1-4] which provides the incentive for

preparing the intrafibrillarly silicifying naturally-calcified collagen matrices. The results of the present study confirmed that demineralized fish scale or bovine bone collagen template can be remineralized via a biomimetic silicification procedure, producing novel silica-base materials with complex hierarchical structure. Apart from the functional similarities in adopting collagen as a mineralization template, the overall mineralization principle also appears to be utilized in both silicification and calcification of hard tissue collagen. During biomineralization, organisms typically accumulate amorphous mineral precursors from their environments, and synthesize biominerals via a bottom-up approach under the control of biomacromolecules.[1,26] Biosilica, found in single cell organisms through higher order plants and primitive animals (sponges), is directed by different organic molecules.[26-29] For sponges and diatoms, silicateins, silaffins and polyamines are thought to be essential for the formation of siliceous skeletons,[28,29] via a phase separation process in the presence of phosphate or other polyvalent anions.[30,31] During the formation of these siliceous structures, silicic acid is thought to be stabilized in a liquid state.[31,32] Different kinds of silaffin or polyamine analogs have been found to stabilize silicic acid as “soluble” silica particles,[33-35] with the positively-charged polyamine interacting with negatively-charged silicic acid to produce an agglutinated “liquid precipitate”.[34,35] In the present work, the PAH-SA appears to be plastic prior to infiltration into the collagen fibrils. This phenomenon is akin to the PILP process involved in biomimetic calcification, wherein amorphous calcium carbonate or calcium phosphate is stabilized by biomimetic analogs of noncollagenous proteins.[7,36] The plasticity of liquid amorphous mineral precursors allows them to take the shape of their containers.[36] Thus, it is likely that a similar mechanism involving the use of polymer-stabilized, plastic, amorphous mineral phases is utilized by Nature in both biocalcification and biosilicification. This accounts for the ability to replace carbonated apatite in fish scales and bovine bone with amorphous silica. The PAH molecule probably stabilizes silicic acid by formation of hydrogen bonds between the silanol groups and amine groups, or by masking the active silanol group with their long polymer chains.[35] Reduction in the availability of $\equiv$Si-O$^-$ anions that are active in nucleophilic reaction with monomeric $Si(OH)_4$ results in inhibition of silicic acid condensation into silica.[34,35] Unlike the negative charges exhibited by polyaspartic acid-stabilized calcium phosphate in biomimetic calcification,[7] the PAH-SA has a highly positive charge (39.4±3.0 mV). The PAH-SA may react with the negatively-charged domains along the collagen fibril surface and subsequently infiltrate into the intrafibrillar spaces of the fibril. As the PAH-SA precursors infiltrate into the collagen fibrils, they interact with hydroxyl groups of the collagen triple helix, resulting in phase separation of the PAH into macromolecular assemblies. Solidification of the siliceous precursors is probably caused by PAH-mediated catalytic conversion of polysilicic acid into silica.[31,37]

To understand the effect of biomimetic silicification on the mechanical properties of collagen, the dynamic mechanical behavior of mineralized, demineralized, and silicified bovine compact bone was investigated with nanoscopical Dynamic Mechanical Analysis indentations (Table I). After demineralization, the complex modulus (E*; sum of the in- and out-of-phase components), storage modulus (E’; elastic response of a material, in-phase component), and loss modulus (E”; viscous response of a material, out-of-phase component) of the bone specimens decreased significantly ($P < 0.05$) due to the loss of minerals.[38] Upon subsequent silicification, E*, E’, and E” significantly increased, compared with the demineralized bone specimens ($P<0.05$). This is attributed to the increased mineral content, as well as recovery of the intermolecular interactions between collagen molecules and intrafibrillar silica.[39] However, those modulus values were still lower than their calcified bone counterparts ($P<0.05$). This may due to incomplete filtration, lack of interfibrillar mineral deposition, reduced coherence between mineral domains during remineralization of the demineralized collagen scaffolds with amorphous silica. The tanδ values (damping – ability of a material to absorb energy) of silicified bone was significantly higher than that of

mineralized bone ($P < 0.05$). Although silicified bone is not as stiff as the calcified bone, it has much higher energy dissipation capability. This unique property enables the highly-resilient silicified collagen matrix to be compressed and re-expand, without causing brittle fracture.

4. CONCLUSION

Results of the present work demonstrate that it is possible for naturally-calcified biominerals to be remineralized by amorphous silica by replacing the carbonated apatite crystallites with an intrafibrillar amorphous silica phase, producing interpenetrating arrangement of collagen-silica composites with unique hierarchical structures. It is speculated that the templating function of collagen matrix and the adoption of liquid precursor mineral phases are shared in both biomimetic silicification and calcification. Due to these similarities, hybrid intrafibrillar silica-apatite-collagen multiphase biomaterials may also be produced, and will be reported in a separate work.

Supplementary Material

Refer to Web version on PubMed Central for supplementary material.

Acknowledgments

We thank Michelle Barnes for secretarial support and Frankie Chan for the University of Hong Kong for his help in STEM-EDX.

Funding Sources This work was supported by grant R01 DE015306-06 from NIDCR (PI. David Pashley), ESA and IPPRM from Georgia Regents University (PI. Franklin Tay), National Nature Science Foundation of China grant 81130078 and National Key Basic Research Program of China grant 2012CB526704 (PI. Ji-hua Chen).

REFERENCES

(1). Ehrlich, H. Biologically-Inspired Systems. Springer; Dordrecht Heidelberg London New York: 2010. Biological Materials of Marine Origin: Invertebrates; p. 25-122.

(2). Wang X, Schröder HC, Wiens M, Ushijima H, Müller WE. Curr. Opin. Biotechnol. 2012; 23:570–578. [PubMed: 22366413]

(3). Müller WE, Wang X, Cui FZ, Jochum KP, Tremel W, Bill J, Schröder HC, Natalio F, Schlossmacher U, Wiens M. Appl. Microbiol. Biotechnol. 2009; 83:397–413. [PubMed: 19430775]

(4). Weiner S, Nudelman F, Sone E, Zaslansky P, Addadi L. Biointerphases. 2006; 1:12–14.

(5). Olszta MJ, Cheng X, Jee SS, Kumar R, Kim YY, Kaufman MJ, Douglas EP, Gower LB. Mater. Sci. Eng. R-Rep. 2007; 58:77–116.

(6). Ehrlich H, Deutzmann R, Brunner E, Cappellini E, Koon H, Solazzo C, Yang Y, Ashford D, Thomas-Oates J, Lubeck M, Baessmann C, Langrock T, Hoffmann R, Wörheide G, Reitner J, Simon P, Tsurkan M, Ereskovsky AV, Kurek D, Bazhenov VV, Hunoldt S, Mertig M, Vyalikh DV, Molodtsov SL, Kummer K, Worch H, Smetacek V, Collins MJ. Nat. Chem. 2010; 2:1084–1088. [PubMed: 21107374]

(7). Nudelman F, Pieterse K, George A, Bomans PH, Friedrich H, Brylka LJ, Hilbers PA, de With G, Sommerdijk NA. Nat. Mater. 2010; 9:1004–1009. [PubMed: 20972429]

(8). Weiher F, Schatz M, Steinem C, Geyer A. Biomacromolecules. 2013; 14:683–687. [PubMed: 23363425]

(9). Niu LN, Jiao K, Qi YP, Yiu CK, Ryou H, Arola DD, Chen JH, Breschi L, Pashley DH, Tay FR. Angew. Chem. Int. Ed. Engl. 2011; 50:11688–11691. [PubMed: 21983995]

(10). Shopsowitz KE, Qi H, Hamad WY, Maclachlan MJ. Nature. 2010; 468:422–425. [PubMed: 21085176]

(11). Van Opdenbosch D, Fritz-Popovski G, Paris O, Zollfrank C. J. Mater. Res. 2011; 26:1193–1202.

(12). Kaehr B, Townson JL, Kalinich RM, Awad YH, Swartzentruber BS, Dunphy DR, Brinker CJ. Proc. Natl. Acad. Sci. U. S. A. 2012; 109:17336–17341. [PubMed: 23045634]

(13). Zylberberg L, Nicolas G. Cell. Tissue Res. 1982; 223:349–367. [PubMed: 7066978]

(14). Beniash E. Wiley Interdiscip Rev. Nanomed. Nanobiotechnol. 2011; 3:47–69. [PubMed: 20827739]

(15). Bruet BJ, Song J, Boyce MC, Ortiz C. Nat. Mater. 2008; 7:748–756. [PubMed: 18660814]

(16). Marino Cugno Garrano A, La Rosa G, Zhang D, Niu LN, Tay FR, Majd H, Arola D. J. Mech. Behav. Biomed. Mater. 2012; 7:17–29. [PubMed: 22340681]

(17). Ehrlich H, Heinemann S, Heinemann C, Simon P, Bazhenov VV, Shapkin NP, Born R, Tabachnick KR, Hanke T, Worch H. J. Nanomater. 2008; 2008:1–8.

(18). Lin CC, Ritch R, Lin SM, Ni MH, Chang YC, Lu YL, Lai HJ, Lin FH. Eur. Cell Mater. 2010; 19:50–57. [PubMed: 20186665]

(19). Aizenberg J, Weaver JC, Thanawala MS, Sundar VC, Morse DE, Fratzl P. Science. 2005; 309:275–278. [PubMed: 16002612]

(20). Wang L, An X, Xin Z, Zhao L, Hu Q. J. Food Sci. 2007; 72:E450–455. [PubMed: 17995604]

(21). Li N, Niu LN, Qi YP, Yiu CK, Ryou H, Arola DD, Chen JH, Pashley DH, Tay FR. Biomaterials. 2011; 32:8743–8752. [PubMed: 21864897]

(22). Almeida RM, Pantano CG. SPIE. 1990; 1328:329–337.

(23). Galeener FL. Phys. Rev. B. 1979; 19:4292–4297.

(24). Luckarift HR, Spain JC, Naik RR, Stone MO. Nat. Biotechnol. 2004; 22:211–213. [PubMed: 14716316]

(25). Haberko K, Bucko MM, Brzezinska-Miecznik J, Haberko M, Mozgawa W, Panz T, Pyda A, Zarębski J. J. Eur. Ceram. Soc. 2006; 26:537–542.

(26). Perry CC. Prog. Mol. Subcell. Biol. 2009; 47:295–313. [PubMed: 19198783]

(27). Currie HA, Perry CC. Ann. Bot. 2007; 100:1383–1389. [PubMed: 17921489]

(28). Shimizu K, Cha J, Stucky GD, Morse DE. Proc. Natl. Acad. Sci. U. S. A. 1998; 95:6234–6238. [PubMed: 9600948]

(29). Kröger N, Deutzmann R, Sumper M. Science. 1999; 286:1129–1132. [PubMed: 10550045]

(30). Wang X, Schloßmacher U, Wiens M, Batel R, Schröder HC, Müller WE. FEBS J. 2012; 279:1721–1736. [PubMed: 22340505]

(31). Kröger N, Lorenz S, Brunner E, Sumper M. Science. 2002; 29:584–586. [PubMed: 12386330]

(32). Schröder HC, Natalio F, Shukoor I, Tremel W, Schlossmacher U, Wang X, Müller WEG. J. Struct. Biol. 2007; 159:325–334. [PubMed: 17336092]

(33). Spinde K, Pachis K, Antonakaki I, Paasch S, Brunner E, Demadis KD. Chem. Mater. 2011; 23:4676–4687.

(34). Sumper M. Angew. Chem. Int. Ed. Engl. 2004; 43:2251–2254. [PubMed: 15108135]

(35). Annenkov VV, Danilovtseva EN, Pal'shin VA, Aseyev VO, Petrov AK, Kozlov AS, Patwardhan SV, Perry CC. Biomacromolecules. 2011; 12:1772–1780. [PubMed: 21469744]

(36). Olszta MJ, Douglas EP, Gower LB. Calcif. Tissue Int. 2003; 72:583–591. [PubMed: 12616327]

(37). Kröger N, Poulsen N. Annu. Rev. Genet. 2008; 42:83–107. [PubMed: 18983255]

(38). Bala Y, Depalle B, Douillard T, Meille S, Clément P, Follet H, Chevalier J, Boivin G. J. Mech. Behav. Biomed. Mater. 2011; 4:1473–1482. [PubMed: 21783157]

(39). Fantner GE, Hassenkam T, Kindt JH, Weaver JC, Birkedal H, Pechenik L, Cutroni JA, Cidade GA, Stucky GD, Morse DE, Hansma PK. Nat. Mater. 2005; 4:612–616. [PubMed: 16025123]

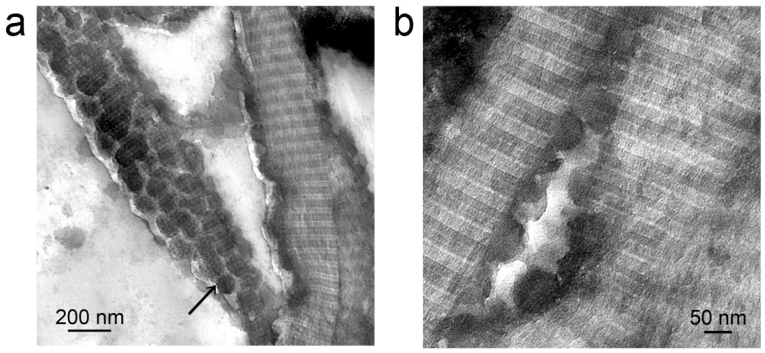

Figure 1. Infiltration of PAH-stabilized silicic acid (PAH-SA) precursors into collagen fibrils

a. Low (bar = 200 nm) and **b**. High magnification (bar = 50 nm) of PAH-SA silicified collagen fibrils. The PAH-SA precursor attached to the surface of the collagen fibrils (black arrow in Fig. a) and infiltrated the intrafibrillar spaces (Fig. b). The hemispherical silica precursors in Fig. b are indicative of the fluidic nature of the soluble PAH-SA precursors.

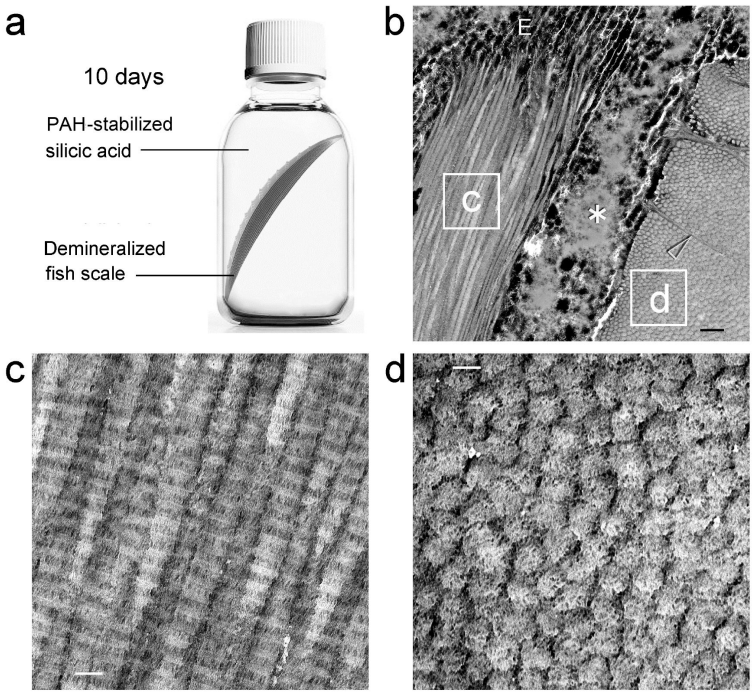

Figure 2. Unstained TEM of biomimetic silicification of completely-demineralized fish scales

a. Schematic representation of biomimetic silicification of fish scale collagen. Completely-demineralized fish scales are infiltrated with poly(allylamine)-stabilized silicic acid. **b.** Two highly-silicified plies of fish scale collagen. Fibrils in ply “c” are arranged 90° to those in ply “d”. The two plies separated during laboratory processing, revealing a highly-silicified edge (E), and inter-ply silica deposits (asterisk). Transversal canals (arrowhead) act as channels for transportation of the silicifying medium into the closely-approximated collagen fibrils (bar = 500 nm). **c.** High magnification of the labeled box “c”. Longitudinal sections of heavily-silicified collagen fibrils reveal intrafibrillar silica deposits that replicate the hierarchical D-spacing of fibrillar collagen (bar = 100 nm). **d.** High magnification of the labeled box “d”. Intrafibrillar silica nanoparticles can be identified within the cross sections of heavily-silicified collagen fibrils (bar = 100 nm).

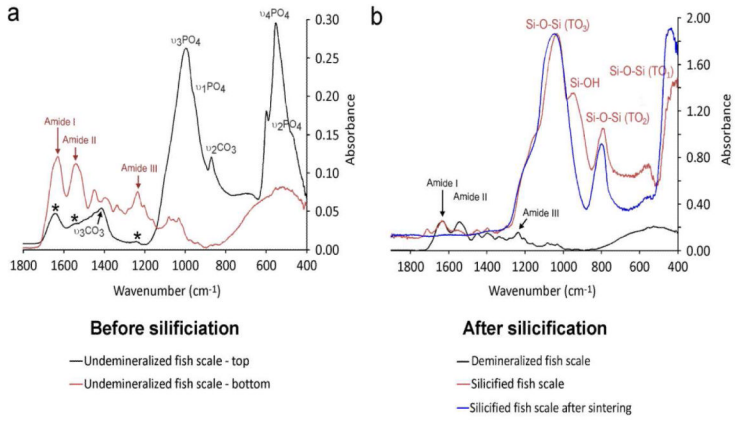

Figure 3. FTIR of fish scales before and after silicification

a. Superimposed infrared spectra of the top (black) and bottom (red) parts of fish scales. **b.** Superimposed infrared spectrum of demineralized fish scale (black), silicified fish scale (red) and silicified fish scale after sintering (blue). All spectra were taken from the top of the fish scales. There is no difference in the infrared spectrum between the top and bottom parts of demineralized fish scale, silicified fish scale and silicified fish scale after sintering (data not shown).

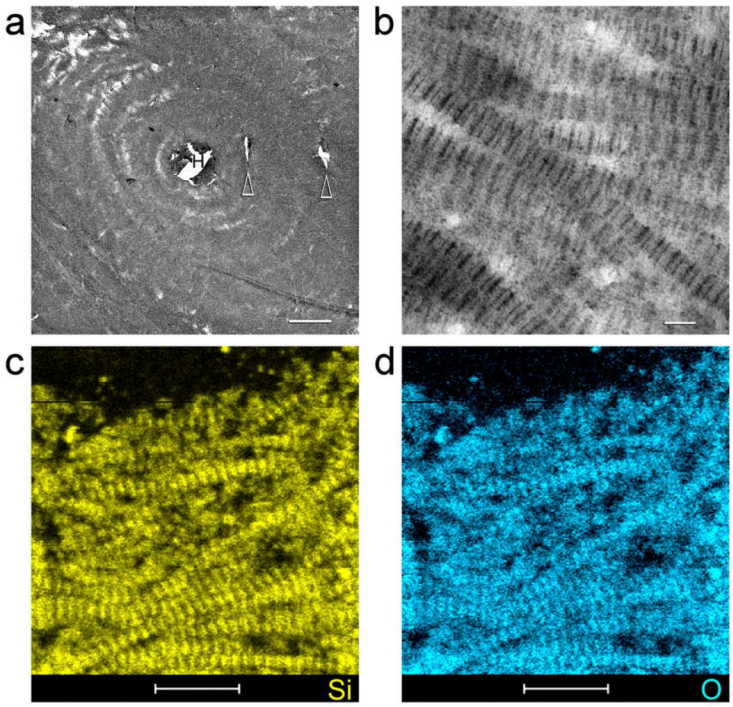

Figure 4. TEM imaging and STEM-EDX of an unstained, non-osmicated section of silicified bovine cortical bone

a, Low magnification TEM of a silicified osteon. The bone matrix was silicified evenly by PAH-stabilized silicic acid delivered via Haversian canal (H) in the centre of the osteon and its interconnecting branches (arrowheads) (bar = 10 μm). **b**, High magnification of the interwoven, silicified collagen fibrils within the osteon, showing cross-banding features created by the intrafibrillar amorphous silica within the collagen fibrils (bar = 100 nm). STEM-EDX elemental mappings indicate the distribution of silicon (**c**) and oxygen (**d**) within the collagen fibrils. The banded appearance of the collagen fibrils was reproduced by the hierarchical distribution of intrafibrillar silica (bar = 500 nm). Calcium and phosphorus were absent from the silicified collagen matrix.

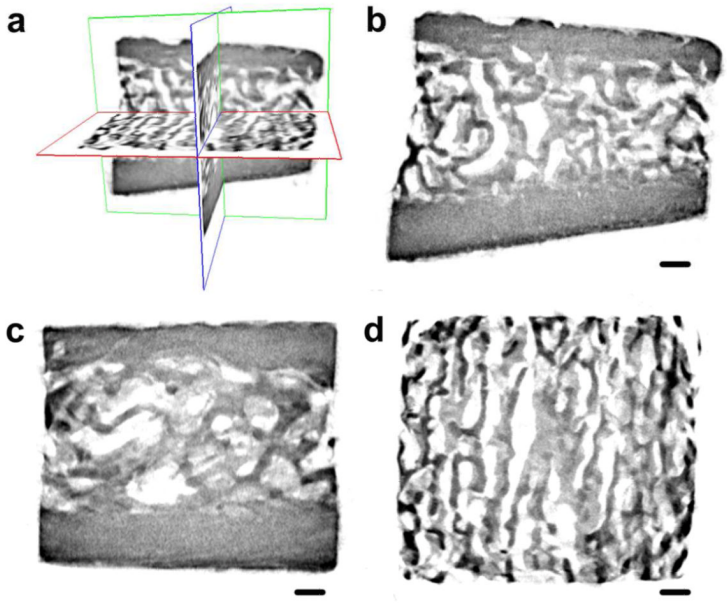

Figure 5. Reconstructed micro-computed tomography images from a silicified bovine bone sample

a. Three-dimensional visualization of the silicified bovine bone; **b.** Coronal image reveals silicification of both compact bone and trabecular bone; **c**. Sagittal image; **d**. Transaxial image reveals the porosities within the silicified trabecular bone (bar = 500 μm).

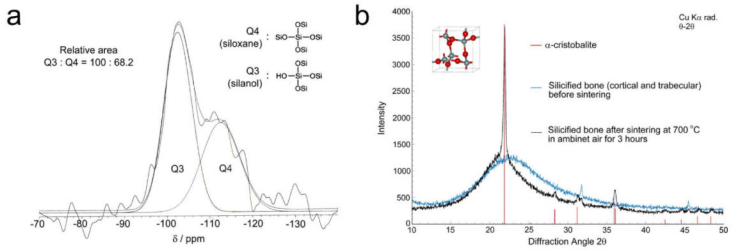

Figure 6. NMR and XRD of silicified PAH-enriched bone matrices

a. $^{1}H \rightarrow ^{29}Si$ CP-MAS NMR spectrum. Deconvolution of the broad peak between −90 and −125 ppm resulted in the resolution of the Q4 (siloxane) peaks at ~110 ppm and the Q3 (single silanol) peak at ~100 ppm. **b**. XRD patterns of silicified bone matrices. Before sintering, the mineral phase is amorphous in nature. After sintering at 700 °C for 3 hours, the amorphous mineral phase was partially converted into crystalline silica (cristobalite; JCPDS file 39-1425).

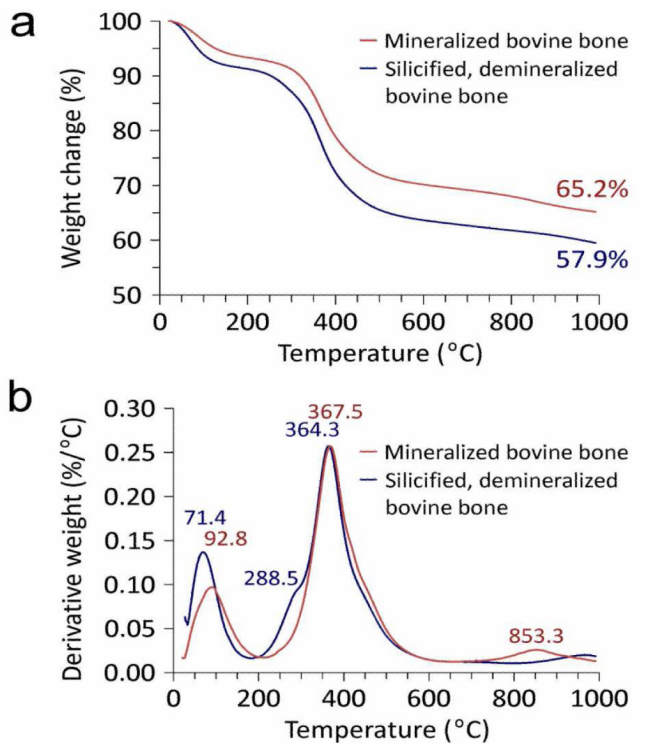

Figure 7. TGA of mineralized bovine bone *vs* silicified bovine bone

a. Plot of weight loss *vs* temperature. **b.** Plot of derivative weight *vs* temperature.

Table 1

Dynamic mechanical properties of mineralized, silicified, and demineralized, hydrated bovine compact bone

	Mineralized bone	Silicified bone	Demineralized bone
E* (GPa)	16.11 ± 1.20[a]	6.95 ± 1.45[b]	0.69 ± 0.11[c]
E' (GPa)	15.56 ± 1.16[a]	6.77 ± 1.43[b]	0.60 ± 0.10[c]
E" (GPa)	0.81 ± 0.21[a]	0.59 ± 0.11[b]	0.10 ± 0.02[c]
Tanδ	0.052 ± 0.013[a]	0.088 ± 0.013[b]	0.164 ± 0.016[c]

Note: For each parameter, groups designated by the same lower case letter are not statistically significant (One-way ANOVA and Holm-Sidak post-hoc multiple comparisons; P > 0.05). E*: Complex modulus; E': Storage modulus; E": Loss modulus.